# Autocorrelation functions for phase separation in ternary mixtures

Sanjay Puri and Deepak Kumar
*School of Physical Sciences, Jawaharlal Nehru University, New Delhi, 110067, India*
(Received 12 May 2004; published 3 November 2004)

We present numerical and analytical results for the autocorrelation functions which characterize domain growth in ternary mixtures. The numerical results are obtained from Monte Carlo simulations of the spin-1 Blume-Emery-Griffiths model with spin-exchange kinetics. Further, we model the autocorrelation functions using an approach based on the continuous-time random walk formalism. The aging property of these functions is related to the time dependence of the domain-size distribution. Our analytical results are found to be in good agreement with the numerical data.

DOI: 10.1103/PhysRevE.70.051501 PACS number(s): 64.75.+g

## I. INTRODUCTION

A homogeneous multicomponent mixture becomes thermodynamically unstable when it is quenched below the coexistence curve. The subsequent far-from-equilibrium evolution of the system is characterized by the emergence and growth of domains enriched in competing phases. For a wide class of systems, domain growth occurs in a scale-invariant manner [1–4]. For example, the time-dependent correlation function exhibits a dynamical-scaling behavior [5]:

$$C(\vec{r},t) = \frac{1}{V}\int d\vec{R}[\langle \psi(\vec{R},t)\psi(\vec{R}+\vec{r},t)\rangle - \langle \psi(\vec{R},t)\rangle\langle \psi(\vec{R}+\vec{r},t)\rangle] \tag{1}$$

$$\equiv g\left(\frac{r}{L(t)}\right), \tag{2}$$

where $\psi(\vec{r},t)$ is the order parameter (e.g., local magnetization for a ferromagnet, density difference of two species for a binary mixture, etc.) at space point $\vec{r}$ and time $t$ after the quench. In Eq. (1), $V$ is the system volume and the angular brackets denote an averaging over independent initial conditions $\psi(\vec{r},0)$ and thermal fluctuations. Equation (2) implies that the morphology of the domain structure remains invariant with time, except for a change in the length scale $L(t)$, which grows with time.

The domain growth or coarsening process is characterized by the time dependence of the length scale $L(t)$, and the functional form of the universal function $g(x)$. These properties depend upon the following factors: (a) the nature of defects in the evolving system, e.g., interfaces, vortices, monopoles, etc., (b) the conservation laws obeyed by the order parameter(s), (c) the presence of hydrodynamic flow fields, and (d) the presence of experimentally relevant effects like quenched or annealed disorder, gravitational fields, internal strain fields in binary alloys, wetting surfaces, etc.

For pure and isotropic systems with a scalar order parameter, the domain growth laws are well understood. Systems with a nonconserved order parameter, e.g., ordering ferromagnets, obey the Lifshitz-Allen-Cahn (LAC) law $L(t) \sim t^{1/2}$ [6]. On the other hand, systems with a conserved order parameter, e.g., phase-separating binary mixtures, are characterized by the Lifshitz-Slyozov (LS) law $L(t) \sim t^{1/3}$ [7].

It is natural to ask whether there are other properties of nonequilibrium systems which exhibit universal features. In this context, a property that has been investigated is the autocorrelation function

$$A(t,t_w) = \frac{1}{V}\int d\vec{R}[\langle \psi(\vec{R},t_w)\psi(\vec{R},t_w+t)\rangle - \langle \psi(\vec{R},t_w)\rangle\langle \psi(\vec{R},t_w+t)\rangle]. \tag{3}$$

In Eq. (3), the times $t_w$ and $(t_w+t)$ are measured subsequent to the quench—$t_w$ is the reference point for measurement of the autocorrelation function, and is referred to as the *waiting time*. [The most general correlation function corresponds to unequal space and time, and combines the definitions in Eqs. (1) and (3).] Equilibrium systems are stationary and the corresponding $A(t,t_w)$ depends only upon the time difference $t$. However, for nonequilibrium systems, the autocorrelation function depends on both $t$ and $t_w$.

The $t_w$ dependence of $A(t,t_w)$ and other response functions has been referred to as the *aging property*. Aging has been extensively discussed in the context of domain-growth kinetics [2], and the nonequilibrium evolution of glassy polymers [8–10] and spin glasses [11,12]. In these systems, the relaxation dynamics becomes progressively slower with the age $t_w$, i.e., there is a $t_w$-dependent increase in the time scale. The simplest possibility in this context is that physical quantities like the autocorrelation function exhibit scaling as

$$A(t,t_w) = h\left(\frac{t}{t_w}\right), \tag{4}$$

where $h(x)$ is the scaling function. Several experimental and numerical studies on, e.g., spin glasses [11–14] are consistent with Eq. (4).

This paper studies the autocorrelation functions for domain growth in ternary (*ABV*) mixtures, modeled by the spin-1 Blume-Emery-Griffiths (BEG) model [15]. The BEG model describes several physical situations, e.g., the superfluid transition in $^3$He-$^4$He mixtures, magnetic transitions in dilute ferromagnets, ternary alloys, etc. [16–19]. Here, we present detailed numerical results for $A(t,t_w)$ in the BEG model with conserved kinetics. Furthermore, we formulate

 

an approach based on the *continuous-time random walk* (CTRW) formalism to understand the behavior of the autocorrelation functions. A summary of our analytical results and representative numerical results were presented in an earlier Letter [20].

This paper is organized as follows. In Sec. II, we present an overview of relevant results. In Sec. II, we also discuss mean-field (MF) phase diagrams for the BEG model at parameter values relevant to our simulations. In Sec. III, we present numerical results from Monte Carlo (MC) simulations of the conserved BEG model. Section IV describes the details of our CTRW modeling, and makes a comparison between the analytical and numerical results for the autocorrelation function. Some of the mathematical details relevant to Sec. IV are relegated to an Appendix. Finally, Sec. V concludes this paper with a summary and discussion of our results.

## II. OVERVIEW OF RELEVANT RESULTS

The spin-1 BEG Hamiltonian for a set of $N$ spins $\{s_i\}$ is as follows [18]:

$$H = -J\sum_{\langle ij\rangle} s_i s_j - K\sum_{\langle ij\rangle} s_i^2 s_j^2 - \frac{M}{2}\sum_{\langle ij\rangle}(s_i^2 s_j + s_i s_j^2) - h\sum_{i=1}^{N} s_i - \Delta\sum_{i=1}^{N} s_i^2, \quad s_i = 0, \pm 1. \tag{5}$$

Here, the interactions are between nearest-neighbor pairs $\langle ij\rangle$ only. The interpretation of various parameters has been discussed extensively in the literature. In the context of dilute magnets, $K$ and $J$ are interactions between atoms and their moments, respectively; $h$ is an external magnetic field; and $\Delta$ is the chemical potential. We consider the case with $J>0$ and $M=0$. The BEG model exhibits a rich phase diagram, which has been extensively explored by a variety of techniques [15–19]. There are four relevant ensembles, corresponding to fixed values of either $h$ or $\Sigma_i s_i$, in conjunction with fixed values of either $\Delta$ or $\Sigma_i s_i^2$.

For ternary ($ABV$) mixtures, the three spin states can be identified with the three components, e.g., $s_i=+1,-1,0$ correspond to $A$, $B$, $V$ atoms, respectively. [We deliberately designate the third component as $V$, because most studies of domain growth in ternary mixtures have focused on binary ($AB$) mixtures with vacancies ($V$) [21–25]. Of course, the discussion here is relevant to arbitrary ternary mixtures.] Then, the parameters in Eq. (5) are related to the energies $\epsilon_{\alpha\beta}$ associated with a nearest-neighbor $\alpha\beta$ pair [26]. Further, the relevant ensemble for discussion of the ternary mixture is one with fixed $\Sigma_i s_i$ and $\Sigma_i s_i^2$.

The BEG model has two order parameters given by $m=\langle s_i\rangle$ and $\rho=\langle s_i^2\rangle$. For a discussion of the phase diagram of the model, we shall employ the dilute magnet interpretation, in which one has a mixture of magnetic atoms (with $s_i=\pm 1\equiv A$ or $B$) and nonmagnetic atoms or vacancies (with $s_i=0\equiv V$). This corresponds to a situation with fixed $h$ and $\Sigma_i s_i^2$. The MF phase diagram of the model in the $(\rho,T)$ plane is shown in Fig. 1 for $h=0$ and $K=1.5,0.5,-1.0$. (All energy scales are measured in units of $J$.) Regions in the phase diagram are marked as $P$, $F$, and 3-phase. Here, $P$ is the paramagnetic phase at high temperatures and low $\rho$ (or high vacancy concentration). Further, $F$ is the ferromagnetic phase which has $A$-rich and $B$-rich domains with $V$ homogeneously distributed in the two phases. In the 3-phase region, there is phase separation between a $V$-rich phase and a magnetic-atom-rich phase. The latter phase consists of $A$-rich (up) and $B$-rich (down) domains. In the 3-phase region, one can distinguish two types of morphologies, depending on the value of $K$ [26]. For $K<1$, vacancies prefer to coat the $AB$ interfaces. We refer to this as the coat ($C$) morphology, where only $AV$ and $BV$ interfaces are present. For $K>1$, the $V$-rich phase forms blobs and $AV$, $BV$, and $AB$ interfaces are all present. We refer to this as the blob ($B$) morphology. The distinction between $B$ and $C$ morphologies is irrelevant at sufficiently large length scales because the coating layer of vacancies in the $C$ morphology saturates at an equilibrium thickness. Subsequent to this saturation, additional vacancies form blobs as this is entropically favorable. The MC simulations reported in Sec. III were done for $K=1.5,0.5,-1.0$, corresponding to Figs. 1(a)–1(c). Other parameter values were $T=0.5$, $m_h=N^{-1}\Sigma_i s_i=0$, and $\rho_h=N^{-1}\Sigma_i s_i^2$

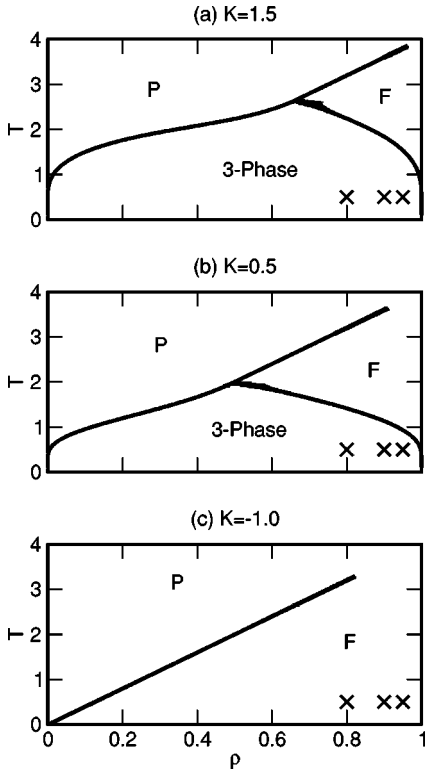


FIG. 1. Mean-field phase diagrams for the spin-1 BEG model in Eq. (5). We consider an ensemble with fixed temperature $T$ and vacancy concentration $c_V=1-\rho$. All parameters are measured in units of $J$, and we set $M=h=0$. The phases are labeled as $P$ (paramagnetic), $F$ (ferromagnetic), and 3-Phase, corresponding to a segregation into a $V$-rich $P$ phase and a $V$-poor $F$ phase. The phase diagrams correspond to (a) $K=1.5$, (b) $K=0.5$, and (c) $K=-1.0$. The parameter values for our MC simulations were $T=0.5$ and $c_V=0.05,0.1,0.2$ (or $\rho=0.95,0.9,0.8$), and are marked as $\times$'s in (a)–(c).

$=0.95, 0.9, 0.8$. (The subscript $h$ refers to the homogeneous state at high temperatures.) These parameter values are marked as $\times$'s in the phase diagrams of Figs. 1(a)–1(c).

In earlier papers, we have investigated the ordering kinetics of the BEG model with nonconserved order parameters [27] as well as conserved order parameters [26]. In Ref. [27], we considered a constrained spin-flip kinetics where $s_i = \pm 1 \rightarrow \mp 1$ only through the state $s_i = 0$. Large values of $\Delta$ $(>0)$ created a barrier to domain growth, and ensured that the spin spent very little time in the state $s_i = 0$. This allowed us to formulate a dichotomic (two-state) CTRW model for computing the autocorrelation function. The analytical results obtained from this stochastic model were in excellent agreement with the corresponding numerical results.

In Ref. [26], we considered spin-exchange kinetics which is appropriate to a ternary mixture. Again, we imposed the above constraint, permitting only $V$-mediated interchanges of the type $A \leftrightarrow V$ and $B \leftrightarrow V$ [21–25]. For this model, we studied the kinetics of phase separation for the blob $(B)$, coat $(C)$, and dispersed $(D)$ morphologies. The $D$ morphology corresponds to the $F$ region in Fig. 1, and consists of $A$-rich and $B$-rich domains with $V$ uniformly dispersed in the system. For all three morphologies, we demonstrated the dynamical scaling of the correlation function $C(r,t) = g(r/L)$ and of the domain-size probability distribution $P(l,t) = L^{-1} f(l/L)$, where $l$ is the domain size. Further, we demonstrated that the characteristic domain scale obeyed the LS growth law $L(t) \sim t^{1/3}$, though the time scales were dependent on the morphology. The present paper focuses upon the autocorrelation functions for $V$-mediated phase separation.

There has been considerable discussion in the literature regarding the functional form of the autocorrelation function in domain growth processes. To summarize this discussion, it is relevant to distinguish two contributions to $A(t,t_w)$: (a) the equilibrium or stationary contribution $A_{\rm st}(t)$, which arises from fluctuations in the interior of bulk domains, and (b) the nonequilibrium or aging contribution $A_{\rm ag}(t,t_w)$, which arises from domain-boundary motion.

The quantity $A_{\rm st}(t)$ has been investigated both analytically and numerically in the context of the two-state kinetic Ising model. Small bulk fluctuations can be discussed in a linear approximation, resulting in an exponential decay of the autocorrelation function, $A_{\rm st}(t) \simeq \exp(-t/\tau)$, where $\tau$ is the time scale. However, Huse and Fisher [28] have argued that droplet fluctuations play an important role at moderately high temperatures, and give rise to a stretched-exponential relaxation [29,30]. The Huse-Fisher argument can be summarized as follows. In a domain of (say) up spins, the probability of a fluctuation consisting of a droplet of down spins of size $L$ is proportional to $\exp(-\beta\sigma L^{d-1})$, where $\beta = (k_B T)^{-1}$, $\sigma$ is proportional to the surface tension, and $d$ is the dimensionality. The lifetime of a droplet depends upon its size, and has the form $t \sim L^{1/\phi}$, where $\phi$ is the corresponding growth exponent. The decorrelation arising due to this droplet is then obtained as

$$A_{\rm st}(t) \simeq \exp(-k\beta\sigma t^{\theta}), \tag{6}$$

where $k$ is a constant and the stretching exponent $\theta = (d-1)\phi$. For $\theta > 1$, the contribution of the droplets is irrelevant and one reverts to the exponential form for $A_{\rm st}(t)$. Thus, the Huse-Fisher argument suggests that

$$\theta = \begin{cases} (d-1)\phi, & d < d_c, \\ 1, & d > d_c, \end{cases} \tag{7}$$

where the critical dimension is defined by $(d_c - 1)\phi = 1$.

Subsequently, Takano *et al.* [31] also studied equilibrium fluctuations in the Ising model. These authors obtained the autocorrelation function as the sum of exponentially decaying terms with relaxation rates $\tau$ having a continuous (length-scale-dependent) spectrum of the form $\tau \sim L^{1/\phi}$. They also found that $A_{\rm st}(t)$ exhibits a stretched-exponential behavior, but with a different stretching exponent:

$$\theta = \frac{(d-1)\phi}{(d-1)\phi + 1}. \tag{8}$$

In an attempt to resolve the discrepancy between these two results, Tang *et al.* [32] undertook a detailed study of the Langevin equation for droplet fluctuations. They examined the relaxation spectrum of the corresponding Fokker-Planck equation for noninteracting spherical droplets. Tang *et al.* found results consistent with the heuristic arguments of Huse and Fisher [28].

There have been various attempts to test these predictions numerically. For example, Takano *et al.* [31] undertook MC simulations of the $d=2$ Ising model with nonconserved kinetics, i.e., $\phi = 1/2$. They found results consistent with the stretching exponent $\theta = 1/3$ predicted by their analytical arguments. More extensive MC simulations are due to Ogielski [33], who studied the nonconserved Ising model in $d=2$, 3, 4. On simulation time scales, his results were consistent with stretched-exponential decay in all cases. Further, the stretching exponents were consistent with Eq. (8) rather than Eq. (7). Finally, we mention the work of Graham and Grant [34], who reported results from a MC study (using a damage-spreading algorithm) of the $d=2$ spin-flip Ising model. These authors found results consistent with exponential decay on the time scales of their simulation. However, these correspond to somewhat limited time windows.

Next, consider the aging part of the autocorrelation function $A_{\rm ag}(t,t_w)$, which results from domain-wall motion. Let us focus on the $T=0$ case, where there is no decorrelation due to bulk fluctuations. One expects that the aging dependence comes from the characteristic length scale $L(t)$. By extension of scaling ideas, it has been argued that the autocorrelation function decays with time as [35,2]

$$A_{\rm ag}(t,t_w) = \left[ \frac{L(t_w)}{L(t+t_w)} \right]^{\lambda}, \; L(t+t_w) \gg L(t_w). \tag{9}$$

For power-law domain growth, this is consistent with the scaling form in Eq. (4). The exponent $\lambda$ was first introduced by Fisher and Huse [35] to describe the dynamical evolution of spin glasses. In the present context, it is a nontrivial exponent which characterizes phase ordering systems.

For specificity, we first consider the ordering dynamics of a ferromagnet, which is described by the spin-flip Ising model or its coarse-grained counterpart, the time-dependent Ginzburg-Landau (TDGL) equation. An important result in

this regard is due to Ohta *et al.* (OJK) [36], who proposed a nonlinear transformation to approximately linearize the (zero-temperature) TDGL equation. The OJK theory yields the following expression for the autocorrelation function:

$$A_{\rm ag}(t,t_w) = \frac{2}{\pi}\sin^{-1}\left[\frac{4t_w(t+t_w)}{(t+2t_w)^2}\right]^{d/4}. \quad (10)$$

In the limit $t+t_w \gg t_w$, we have

$$A_{\rm ag}(t,t_w) \simeq \frac{2}{\pi}\left(\frac{4t_w}{t+t_w}\right)^{d/4}. \quad (11)$$

The OJK function in Eq. (10) exhibits the scaling behavior in Eq. (4). Recall that the coarsening ferromagnet obeys the LAC growth law $L(t)\sim t^{1/2}$. Then, Eq. (11) is also seen to be consistent with Eq. (9), and we can identify the exponent $\lambda = d/2$ in the OJK approximation. As a matter of fact, this expression is exact for the TDGL model with $O(n)$ symmetry in the limit $n=\infty$ [2]. Further, the exact value in $d=1$ (where $T_c=0$) is $\lambda=1$ [37,38]. More generally, Fisher and Huse [35] proposed bounds on the value of $\lambda$, viz., $d/2 \leqslant \lambda \leqslant d$. Finally, the value of $\lambda$ has been studied numerically for $d \geqslant 2$ via simulations of the nonconserved Ising model [39].

Our understanding of the conserved case is considerably poorer. Yeung *et al.* (YRD) [40] have obtained the bounds $\lambda \geqslant d/2+2$ for $d \geqslant 2$ and $\lambda \geqslant 3/2$ for $d=1$. (This assumes that $t_w$ is in the scaling regime. For $t_w=0$, YRD argue that $\lambda \geqslant d/2$ for all $d$.) YRD also presented results from simulations of the $d=2$ Cahn-Hilliard equation (without thermal fluctuations), and found that $\lambda \simeq 4$, consistent with their bounds. Another study is due to Marko and Barkema (MB) [41], who undertook MC simulations of the Ising model with spin-exchange kinetics in $d=2$, 3. These authors used an accelerated algorithm to access the asymptotic regime of phase-separation kinetics. MB claim that their data for the autocorrelation function is consistent with a power-law decay as in Eq. (9). However, their numerical data do not validate this conclusion. For example, their plots of $\ln[A(t,t_w)]$ vs $\ln(t+t_w)$ (see Figs. 2 and 5 of Ref. [41]) exhibit a continuous curvature, whereas a power-law decay would correspond to a straight line. It should be noted that their simulations were conducted at nonzero temperatures, so there are contributions to $A(t,t_w)$ from both bulk fluctuations (stretched-exponential type) and domain-wall motion (power-law type). These must be accounted for in any complete description of the autocorrelation function in phase-ordering systems.

The above discussion has focused on domain growth in pure systems. In disordered systems like spin glasses, different features arise due to the multiplicity of metastable states [42,43]. An important study in this context is due to Fisher and Huse (FH) [35], who argue that the two-state Ising spin glass has two unique disordered-looking ground states, which are related by the symmetry transformation $s_i \to -s_i$. In the FH scenario, relaxation at low temperatures proceeds by coarsening of these phases through domain growth. However, domain walls get locally trapped by disorder and their subsequent motion is via thermal activation over length-scale-dependent barriers. The corresponding domain growth law is [35]

$$L(t) \sim \left[\frac{T}{\Delta(T)}\ln\left(\frac{t}{\tau}\right)\right]^{1/\bar{\psi}}, \quad (12)$$

where $\Delta(T)$ is the scale of disorder barriers, $\tau$ is a timescale, and $1/\bar{\psi}$ is the growth exponent. The FH prediction for the autocorrelation function in this case is obtained by replacing Eq. (12) in Eq. (9). Note that this does not result in an aging form with $t/t_w$ scaling.

We should stress that the FH model is still the subject of controversy. An alternative description of spin glasses is the replica-symmetry-breaking (RSB) model of Parisi [44], where there are an infinite number of equivalent ground states. The RSB scenario has been rigorously proven only for the infinite-ranged Sherrington-Kirkpatrick model [45], and its applicability to short-ranged spin glasses remains the subject of much discussion.

## III. DETAILED NUMERICAL RESULTS

Before presenting results, we briefly describe details of our MC simulation techniques. We study ordering dynamics in the $d=2$ BEG model with Kawasaki spin-exchange kinetics. The microscopic kinetics individually conserves numbers of $s_i=0,\pm 1$. Following our earlier work [26], we impose a constraint on the kinetics and allow only vacancy-mediated dynamics. However, we should stress that similar results are obtained for unconstrained kinetics, where all types of interchanges are permitted. This is because the barrier to $A \leftrightarrow B$ interchanges at domain interfaces (i.e., $E_B = 12J$ in $d=2$) is much higher than that for $A \leftrightarrow V$ and $B \leftrightarrow V$ interchanges (i.e., $E_B=6J$ in $d=2$). Thus, especially at low temperatures, the segregation dynamics is primarily driven by $V$'s—regardless of whether or not $A \leftrightarrow B$ interchanges are allowed.

The system size was taken to be $N^2$ (with $N=512$), and periodic boundary conditions were imposed in both directions. The initial condition for the MC simulation consists of a random distribution of $A,B,V$ with number densities $(1-c_V)/2$, $(1-c_V)/2$, $c_V$, respectively. This mimics the high-temperature disordered state prior to the quench. The system is quenched to a low temperature $T$ at time 0. A randomly chosen pair of spins is interchanged according to the above stochastic move, corresponding to a change in configuration from $\{s_i\} \to \{s_i'\}$. The change is accepted with probability $p_a = \exp(-\beta \Delta H)$ if $\Delta H > 0$, or $p_a=1$ if $\Delta H < 0$, where $\Delta H = H(\{s_i'\}) - H(\{s_i\})$ is the change of energy associated with the move [46]. A Monte Carlo step (MCS) corresponds to $N^2$ attempted updates. The results presented here correspond to a random-updating procedure, but similar results were obtained with sequential updates. All statistical data were obtained as an average over ten independent runs.

In contrast to most earlier works [21–25], we have studied physical situations with appreciable $V$ concentrations so as to investigate domain coarsening in both regions of the phase diagram, namely, regions with two-phase and 3-phase coexistence. As mentioned earlier, the parameter values studied are marked as $\times$'s in the phase diagrams of Fig. 1.

We start by showing typical evolution morphologies. Figure 2 shows the evolution pictures for $K=1.5$, 0.5, $-1.0$ and

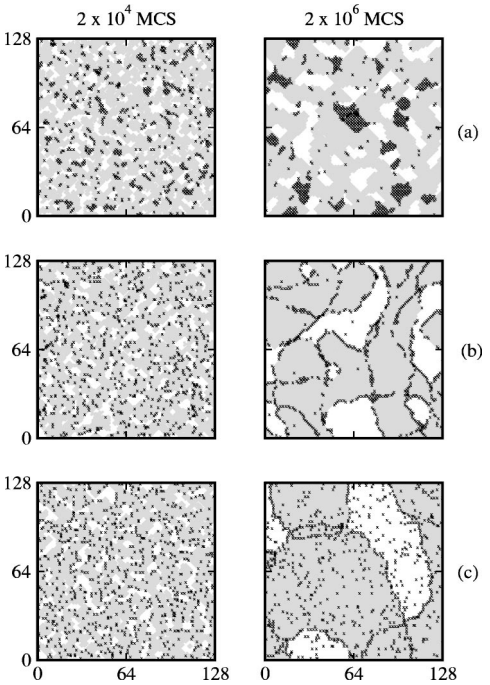


FIG. 2. Evolution pictures obtained from $d=2$ MC simulations of the *ABV* model with *V*-mediated exchange kinetics. The lattice size was $512^2$ and periodic boundary conditions were applied in both directions. (For clarity, the pictures show only a $128^2$ corner of the lattice.) The initial condition for each run consisted of a random mixture of *A*, *B*, and *V* with concentrations $(1-c_V)/2$, $(1-c_V)/2$, and $c_V$, respectively. Snapshots are labeled by the time subsequent to the quench. The *A*-rich and *B*-rich regions are marked in gray and white, and the *V*'s are marked as ×'s. Results are shown for $T=0.5$, $c_V=0.05$, and (a) $K=1.5$ (blob or *B* morphology), (b) $K=0.5$ (coat or *C* morphology), (c) $K=-1.0$ (dispersed or *D* morphology).

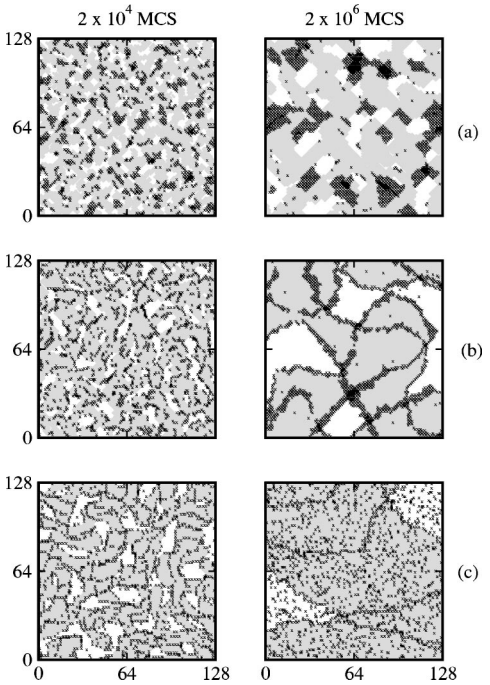


FIG. 3. Analogous to Fig. 2, but for the case $c_V=0.1$.

vacancy concentration $c_V=0.05$. The gray and white regions correspond to *A*-rich and *B*-rich phases, respectively. The crosses denote the vacancies. Panels (a) and (b) arise for quenches in the 3-phase region (see Fig. 1) and correspond to the *B* and *C* morphologies, respectively. Notice the formation of *V* clusters in the gray and white regions in the *C* morphology—these are due to the existence of a *V*-rich phase. Panel (c) corresponds to a quench in the *F* phase, and we see vacancies dispersed uniformly in the up and down domains, corresponding to the *D* morphology. Figure 3 is a similar set of evolution pictures at $c_V=0.1$. The same broad features are observed in these pictures. However, notice that the *C* morphology in panel (b) clearly exhibits *V*-rich blobs at $t=2\times10^6$ MCS, because the *AB* interfaces are already saturated with vacancies.

Next, we discuss our results for the domain-size distribution function $P(l,t)$, which is computed by examining order-parameter profiles along horizontal and vertical cross sections of the lattice [26,27]. We consider here distributions for the *A*-rich and *B*-rich domains. In Ref. [26], we demonstrated that this quantity obeys the dynamical-scaling property, $P(l,t)=L^{-1}f(l/L)$, for all three morphologies. The scaling function is independent of the nature of the morphology. This is seen in Fig. 4, where we superpose data for $P(l,t)L$ vs $l/L$ for the *B*, *C*, and *D* morphologies. The characteristic length scale $L$ is defined from the domain-size distribution function as $L(t)=\langle l\rangle$. We have also superposed data for the two-state spin-exchange Ising model in Fig. 4, and this also coincides well with the scaling function. Clearly, the scaling function is also independent of the *V* concentration. In Fig. 4(b), we plot the data of Fig. 4(a) on a linear-log scale, and observe that the tail of the scaling function is exponential.

Subsequently, the form of the scaling function will be a crucial input in our stochastic modeling. One possibility is to directly use the numerical data for the scaling function from Fig. 4. Alternatively, it is convenient to obtain an empirical form for the function $f(x)$. The solid line in Figs. 4(a) and 4(b) is a best fit to the empirical function

$$f(x)=\frac{a_1x+a_2x^2+a_3x^3}{1+b_1x+b_2x^2+b_3x^3}e^{-cx}. \tag{13}$$

The best-fit parameter values are specified in the figure caption.

Next, we focus on the behavior of the autocorrelation functions, which is our primary interest in the present study. For the kinetic BEG model, we can define the following two functions [cf. Eq. (3)]:

$$A_m(t,t_w)=\frac{1}{N^2}\sum_{i=1}^{N^2}[\langle s_i(t_w)s_i(t_w+t)\rangle-\langle s_i(t_w)\rangle\langle s_i(t_w+t)\rangle] \tag{14}$$

and

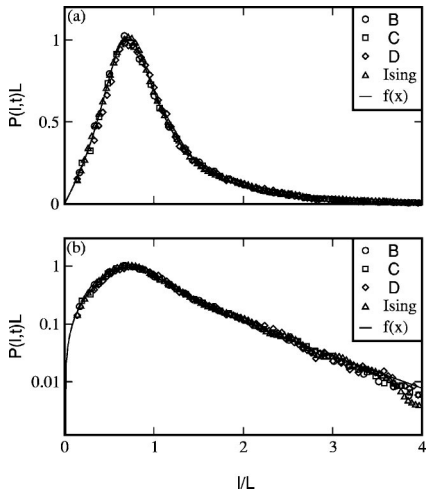


FIG. 4. (a) Scaling plot of the domain-size probability distribution $P(l,t)L$ vs $l/L$, for the evolution depicted in Fig. 3. We consider only *A*-rich and *B*-rich domains here. The probability distribution is computed by examining interface locations along horizontal and vertical cross sections of the lattice. All statistical data are obtained as an average over ten independent runs for $512^2$ lattices. The characteristic length scale $L$ is defined as $\langle l \rangle$, the first moment of the probability distribution. We present data for the *B*, *C*, and *D* morphologies at $t=10^6$ MCS. For comparison, we also present data for the two-state spin-exchange Ising model at $t=10^6$ MCS. The solid line corresponds to the empirical function in Eq. (13). The best-fit parameters are $a_1=1.077$, $a_2=-0.577$, $a_3=0.818$, $c=1.5$, $b_1=-2.245$, $b_2=1.748$, $b_3=0.075$. (b) Data from (a), plotted on a linear-log scale.

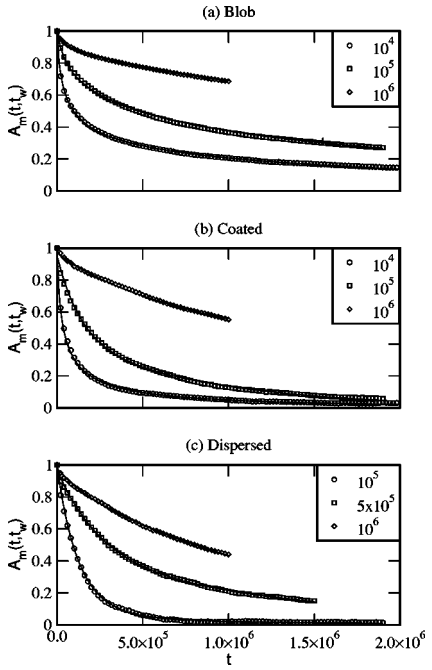


FIG. 5. Time dependence of the autocorrelation function $A_m(t,t_w)$ vs $t$. The autocorrelation function is normalized to unity at $t=0$. The data corresponds to the evolution depicted in Fig. 2 ($c_V=0.05$) with (a) $K=1.5$, waiting times $t_w=10^4,10^5,10^6$; (b) $K=0.5$, $t_w=10^4,10^5,10^6$; (c) $K=-1.0$, waiting times $t_w=10^5,5\times10^5,10^6$. The solid lines correspond to best fits to the functional form in Eq. (25) for (a) and (b), and Eq. (31) for (c). The best-fit parameter values are shown in Table I.

$$A_\rho(t,t_w)=\frac{1}{N^2}\sum_{i=1}^{N^2}[\langle s_i^2(t_w)s_i^2(t_w+t)\rangle-\langle s_i^2(t_w)\rangle\langle s_i^2(t_w+t)\rangle]. \tag{15}$$

We confine ourselves to presenting numerical results for $A_m(t,t_w)$ in the present exposition. The results obtained for $A_\rho(t,t_w)$ are analogous to those presented here. Figure 5 plots $A_m(t,t_w)$ vs $t$ for the *B*, *C*, and *D* morphologies depicted in Fig. 2 (with $c_V=0.05$). Notice that there is a substantial slowing down of the decay of the autocorrelation function with aging. Further, the basic time scales are dependent on the morphology, with *B* and *D* exhibiting the slowest and fastest decays, respectively. This is because the density of vacancies available to drive the ordering kinetics depends strongly on the morphology (see Fig. 2). The solid lines superposed on the data sets are fits based on the CTRW modeling of the autocorrelation function, which is discussed in the next section.

In Fig. 6, we plot the data of Fig. 5 on a log-log plot. The data exhibit a continuous curvature and are not consistent with the power-law decay in Eq. (9). As stated earlier, this is because decorrelation occurs due to bulk (equilibrium) fluctuations in conjunction with domain-wall motion. It is also relevant to test whether the autocorrelation function exhibits the scaling form in Eq. (4). In Fig. 7, we plot the data of Fig. 5 on the scaling plot, $A_m(t,t_w)$ vs $t/t_w$. Again, we see that this scaling form is not obeyed by our numerical data, even for large values of $t_w$.

Finally, Fig. 8 is analogous to Fig. 5, but corresponds to the case with $c_V=0.1$ (shown in Fig. 3). Again, the solid lines superposed on the data sets are best fits to the corresponding CTRW result discussed in Sec. IV.

## IV. MODELING THE AUTOCORRELATION FUNCTION

In this section, we propose a CTRW model [47–49] for the spin dynamics and use it to compute the autocorrelation functions. Our stochastic model accounts for both aging and bulk fluctuations, and is based on rather general principles as follows. First, we interpret the single-spin dynamics as a trichotomic Markov process [50,51]. Second, we assume that the time scales involved in the decorrelation of a spin depend on the size of the domain to which the spin belongs. Thus, the $A_m$ and $A_\rho$ as defined in Eqs. (14) and (15) are first obtained for a domain of arbitrary size by the CTRW method, and then averaged over the domain-size distribution function. In our modeling, aging is incorporated through the domain-size distribution function, as the characteristic length scale depends on the aging time.

The details of the stochastic modeling are given in the Appendix. Here, we describe the general formalism and the results obtained from it. Recall that a single spin $s_i(t)$ can be in three possible states with occasional transitions between

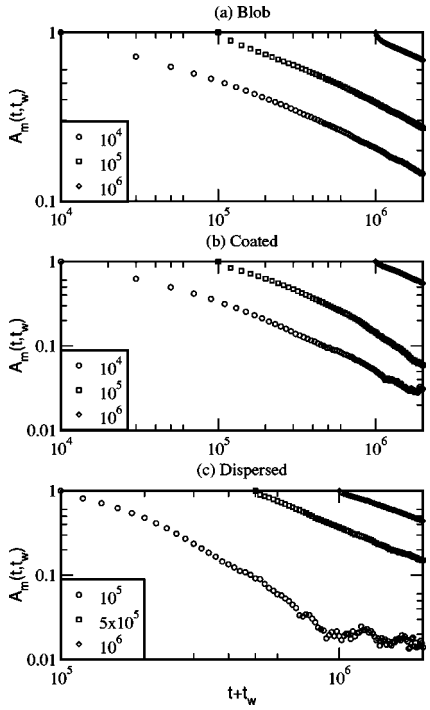


FIG. 6. Data from Fig. 5, replotted as $A_m(t,t_w)$ vs $(t+t_w)$ on a log-log scale.

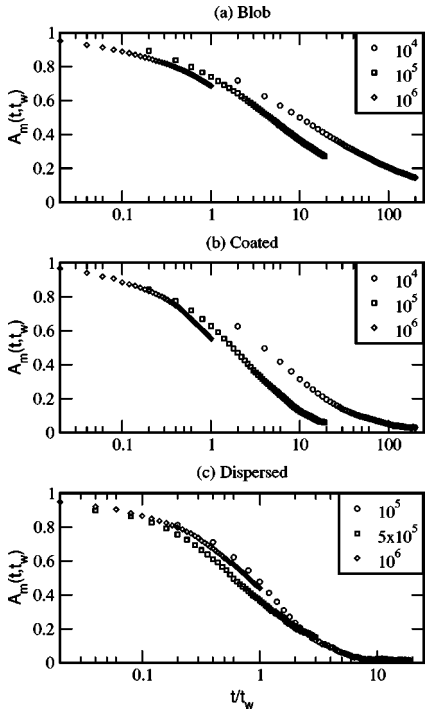


FIG. 7. Data from Fig. 5, replotted as $A_m(t,t_w)$ vs $t/t_w$ on a log-linear scale.

these states. The state of the spin at a given time is described by a probability vector $\vec{P}(t)$, where

$$\vec{P}(t) = \begin{pmatrix} P_+(t) \\ P_0(t) \\ P_-(t) \end{pmatrix}. \tag{16}$$

Here, $P_n(t)$ denotes the probability for the spin to be in state $n(=+1,0,-1)$ at time $t$. The stochastic evolution of this state is described in terms of two matrices: the persistence matrix $\Psi(t)$ and the transition matrix $W(t)$. The persistence matrix describes the probability that, after a transition at $t=0$, the resultant state persists upto time $t$. This involves three waiting-time distributions $\psi_n(t)$, and $\Psi(t)$ is given by

$$\Psi(t) = \begin{pmatrix} \psi_+(t) & 0 & 0 \\ 0 & \psi_0(t) & 0 \\ 0 & 0 & \psi_-(t) \end{pmatrix}. \tag{17}$$

Next, we consider the transition matrix $W(t)$. This gives the probability of a transition at time $t$, given that the last transition occurred at $t=0$. Now, a transition out of the $n$ state in the time interval $[t,t+\Delta t]$ occurs with probability $-\dot{\psi}_n(t)\Delta t$. Given the nature of our dynamics, in which only $\pm 1 \leftrightarrow 0$ interchanges are allowed, we can write the transition matrix as

$$W(t) = -\begin{pmatrix} 0 & \frac{1}{2}\dot{\psi}_0(t) & 0 \\ \dot{\psi}_+(t) & 0 & \dot{\psi}_-(t) \\ 0 & \frac{1}{2}\dot{\psi}_0(t) & 0 \end{pmatrix}. \tag{18}$$

Thus, the stochastic evolution is described in terms of the three $\psi_n(t)$'s. In our modeling, we assume a simple exponential form $\psi_n(t)=\exp(-\gamma_n t)$. One can now use the CTRW formalism to obtain the state of the spin $\vec{P}(t)$ at arbitrary time starting from the state $\vec{P}(0)$, by summing over all possible transitions. The formal result is expressed in terms of an evolution operator as follows:

$$\vec{P}(t) = U(t)\vec{P}(0), \tag{19}$$

as specified in Eqs. (A3)–(A5). This allows us to calculate both $A_m(l,t)$ and $A_\rho(l,t)$ for a domain of size $l$. The calculation of $\vec{P}(t)$ and the corresponding autocorrelation functions is presented in the Appendix.

Let us now adapt these expressions to describe decorrelation in the domain-growth processes depicted in Figs. 2 and 3. Consider a typical domain (say, up) of size $l$. The decorrelation of this domain occurs due to the stochastic evolution of spins in the domain. Due to energetic considerations, the survival times of spins $s_i=+1$, 0, $-1$ in an up domain are related as $\gamma_+^{-1} \gg \gamma_0^{-1} \gg \gamma_-^{-1}$. The opposite relationship holds in a down domain. We associate a two-time-scale exponential autocorrelation function [as in Eq. (A18)] with spins in this domain. However, the time scales are $l$ dependent because the evolution is driven by $V$'s, which are concentrated on the domain boundaries—at least in the $B$ and $C$ phases. Thus, the autocorrelation function for a single up domain of size $l$ is

$$A_m(l,t) \simeq pe^{-\gamma_a(l)t} + (1-p)e^{-\gamma_b(l)t}. \tag{20}$$

Here, the parameter $p$ determines the relative proportion of the two time scales. Due to symmetry, the same expression applies for down domains. Further, the $V$ domains do not contribute to the autocorrelation function. The overall corre-

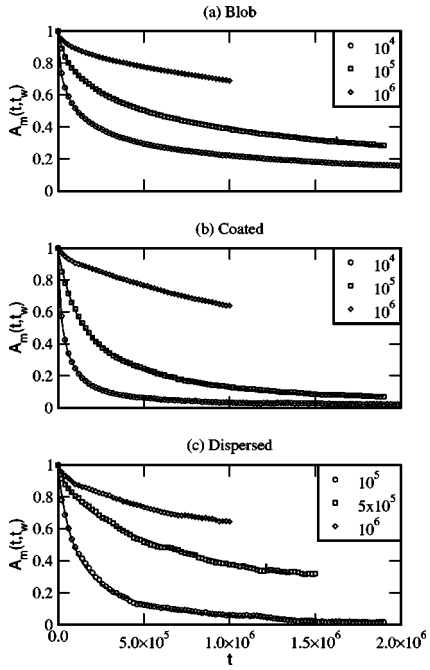


FIG. 8. Analogous to Fig. 5, but for the evolution depicted in Fig. 3 ($c_V=0.1$). The best-fit parameter values are shown in Table II.

lation function is obtained by integrating over the probability distributions of up and down domains as

$$A_m(t) \simeq (1-c_V)\int_0^\infty dl\, P(l,t)[pe^{-\gamma_a(l)t} + (1-p)e^{-\gamma_b(l)t}], \quad (21)$$

where we have set $P_+(l,t)=P_-(l,t)=P(l,t)$ from symmetry considerations.

For the dispersed ($D$) phase, there are no distinct regions of the $V$-rich phase, though there is a coating of the $AB$ interfaces by $V$'s (see Figs. 2 and 3). In that case, the decorrelation of an up domain (or down domain) of size $l$ is obtained as

$$A_m(l,t) \simeq (1-c_V)[pe^{-\gamma_a(l)t} + (1-p)e^{-\gamma_b(l)t}]. \quad (22)$$

The overall correlation function is obtained by integrating over the probability distribution, again yielding the expression in Eq. (21). The generalization of Eq. (21) to mixtures with asymmetric composition, and asymmetric time scales in up and down domains, is straightforward.

The crucial inputs in our stochastic modeling are the functional forms of $\gamma_a(l)$ and $\gamma_b(l)$ for the different morphologies $B$, $C$, and $D$. Let us consider these separately below.

### A. Blob morphology

In the blob morphology, we have $A$-, $B$-, and $V$-rich domains, all in contact with each other (see Figs. 2 and 3). Consider an $A$-rich domain of size $l$ in contact with a $V$-rich domain of size $l_0$. The length of the contact line $l_0 \sim l$, and the fraction of the domain involved in the dynamics $\sim l^{-1}$. Therefore, we expect that

TABLE I. Best-fit parameter values for the autocorrelation functions shown in Fig. 5 (with $c_V=0.05$).

| Morphology | $t_w$ | $\gamma_1\times10^5$ | $\gamma_2\times10^5$ | $p$ |
|---|---|---|---|---|
| Blob | $10^4$ | 6.9 | 68.3 | 0.83 |
| | $10^5$ | 6.2 | 71.4 | 0.78 |
| | $10^6$ | 5.8 | 88.1 | 0.91 |
| Coat | $10^4$ | 19.2 | 81.2 | 0.91 |
| | $10^5$ | 20.4 | 83.3 | 0.94 |
| | $10^6$ | 21.3 | 78.8 | 0.96 |
| Dispersed | $10^5$ | 32.2 | 0.8 | 0.71 |
| | $5\times10^5$ | 34.4 | 0.6 | 0.75 |
| | $10^6$ | 28.6 | 0.7 | 0.83 |

$$\gamma_a(l) \simeq al^{-1}, \quad \gamma_b(l) \simeq bl^{-1}, \quad (23)$$

where $a$, $b$ are constants whose $c_V$ dependence we clarify shortly. Then, Eq. (21) becomes

$$A_m(t) \simeq (1-c_V)\int_0^\infty dl\, P(l,t)[pe^{-at/l} + (1-p)e^{-bt/l}]. \quad (24)$$

Recall the scaling form of the probability distribution $P(l,t)=L^{-1}f(l/L)$, where the characteristic length scale obeys the LS law $L \simeq k(t+t_w)^{1/3}$, with $k$ being a constant. In general, $k$ increases with $c_V$ in a manner which depends on the morphology. Replacing this in the above expression, we obtain ($x=l/L$)

$$A_m(t,t_w) \simeq (1-c_V)\int_0^\infty dx\, f(x)\left[p\exp\left(-\frac{\gamma_1}{x}\frac{t}{(t+t_w)^{1/3}}\right) + (1-p)\exp\left(-\frac{\gamma_2}{x}\frac{t}{(t+t_w)^{1/3}}\right)\right], \quad (25)$$

where $\gamma_1=a/k$, $\gamma_2=b/k$. This is the functional form that the numerical data in Figs. 5(a) and 8(a) were fitted to. The fitting parameters $\gamma_1$, $\gamma_2$, $p$ are specified in Tables I and II. We should make three important observations in this context.

TABLE II. Best-fit parameter values for the autocorrelation functions shown in Fig. 8 (with $c_V=0.1$).

| Morphology | $t_w$ | $\gamma_1\times10^5$ | $\gamma_2\times10^5$ | $p$ |
|---|---|---|---|---|
| Blob | $10^4$ | 7.0 | 68.3 | 0.83 |
| | $10^5$ | 6.1 | 70.2 | 0.78 |
| | $10^6$ | 5.9 | 88.4 | 0.91 |
| Coat | $10^4$ | 17.5 | 90.2 | 0.74 |
| | $10^5$ | 17.2 | 77.4 | 0.71 |
| | $10^6$ | 14.4 | 73.2 | 0.88 |
| Dispersed | $10^5$ | 25.4 | 1.5 | 0.90 |
| | $5\times10^5$ | 18.9 | 2.0 | 0.89 |
| | $10^6$ | 28.0 | 1.8 | 0.91 |

(a) The fitting parameters are seen to be reasonably independent of the waiting time $t_w$, as expected in the above formulation.

(b) One decay rate ($\gamma_1$) is an order of magnitude smaller than the other decay rate ($\gamma_2$). This is a consequence of the very different survival times for different spin types, e.g., $\gamma_+^{-1} \gg \gamma_0^{-1} \gg \gamma_-^{-1}$ in an up domain. In this limit, Eq. (A17) yields $\gamma_a \simeq \gamma_0/2 + \gamma_+$, $\gamma_b \simeq \gamma_- + \gamma_0/2$, so that $\gamma_b \gg \gamma_a$.

(c) The fitting parameters do not show strong dependence on $c_V$. This is because the $V$'s are confined in blobs and their availability only changes marginally with increase in $c_V$. Further, any dependence of the constants $a$, $b$ on $c_V$ is offset by the corresponding $c_V$ dependence of the constant $k$ in the LS growth law.

### B. Coat morphology

The arguments for the coat morphology are analogous to those for the blob morphology, and the final expression for the autocorrelation function is Eq. (25) again. The parameter values corresponding to the best-fits shown for the data sets in Figs. 5(b) and 8(b) are also presented in Tables I and II, respectively. The observations made about parameter values in the context of the $B$ morphology apply in the present case also, with suitable modifications.

It is relevant to understand the behavior of $A_m(t,t_w)$ in the limit $t \to \infty$. Recall that $f(x) \sim e^{-cx}$ for $x \geq 1$ [see Fig. 4(b)]. Thus, the expression in Eq. (25) is determined by integrals of the form

$$I = \int_0^\infty dx\, e^{-cx} \exp\left( - \frac{\gamma_1}{x} \frac{t}{(t+t_w)^{1/3}} \right). \tag{26}$$

We can perform a saddle-point expansion to approximate this integral as

$$I \simeq \left( \frac{\pi^2 \gamma_1}{c^3} \right)^{1/4} \frac{t^{1/4}}{(t+t_w)^{1/12}} \exp\left[ - 2(c\gamma_1)^{1/2} \frac{t^{1/2}}{(t+t_w)^{1/6}} \right], \tag{27}$$

which corresponds to a stretched-exponential with exponent $1/3$. The overall result for $t \to \infty$ is

$$A_m(t,t_w) \sim \left( \frac{\pi^2}{c^3} \right)^{1/4} \frac{t^{1/4}}{(t+t_w)^{1/12}} \times \left[ p\gamma_1^{1/4} \exp\left( - 2(c\gamma_1)^{1/2} \frac{t^{1/2}}{(t+t_w)^{1/6}} \right) + (1-p)\gamma_2^{1/4} \exp\left( - 2(c\gamma_2)^{1/2} \frac{t^{1/2}}{(t+t_w)^{1/6}} \right) \right]. \tag{28}$$

Notice that this result (for $t \gg t_w$) is consistent with the $d=2$ result of Huse and Fisher [28] and Tang *et al.* [32], though it has been arrived at by a different route.

### C. Dispersed morphology

The dispersed morphology is considerably different from the $B$ and $C$ morphologies, as is apparent from Figs. 2 and 3. Notice that the early-time pictures (at $t = 2 \times 10^4$ MCS) do not exhibit the asymptotic dispersed morphology. This is because it is energetically preferable to locate $V$'s at interfaces, if these are available. At later times, the excess $V$'s dissolve into the bulk domains. We will focus on the late-time regime here as it corresponds to the correct asymptotic morphology.

In the dispersed phase, decorrelation occurs due to $V$'s inside bulk domains (with an $l$-independent time scale) and $V$'s on interfaces (with an $l$-dependent time scale). We assume that

$$\gamma_a(l) \simeq a l^{-1}, \quad \gamma_b(l) \simeq b c_V = \gamma_2, \tag{29}$$

where $a$, $b$ are constants. Then, Eq. (25) yields

$$A_m(t,t_w) \simeq (1-c_V) \int_0^\infty dl\, P(l,t) [p e^{-at/l} + (1-p) e^{-\gamma_2 t}]. \tag{30}$$

If we insert the scaling form of $P(l,t)$, we obtain

$$A_m(t,t_w) \simeq (1-c_V) \left[ p \int_0^\infty dx\, f(x) \exp\left( - \frac{\gamma_1}{x} \frac{t}{(t+t_w)^{1/3}} \right) + (1-p) e^{-\gamma_2 t} \right]. \tag{31}$$

The resultant fits are shown in Figs. 5(c) and 8(c), and the corresponding best-fit parameters are specified in Tables I and II. Note that the parameter $\gamma_2$ approximately follows the $c_V$ dependence in Eq. (29), whereas $\gamma_1 \sim k^{-1}$ decreases with increasing $c_V$.

## V. SUMMARY AND CONCLUSION

Let us conclude this paper with a summary and discussion of the results presented here. We have studied the behavior of the autocorrelation functions which characterize domain growth in the BEG model with conserved kinetics. The BEG model describes ternary ($ABV$) mixtures and we focus on the case of $V$-mediated kinetics, i.e., $A \leftrightarrow V$ and $B \leftrightarrow V$ interchanges are allowed but not $A \leftrightarrow B$ interchanges. However, the results obtained for this constrained kinetics are comparable to those arising for unconstrained kinetics. This is because the energy barriers for $A \leftrightarrow B$ interchanges at domain boundaries are much higher than those for $A, B \leftrightarrow V$ interchanges.

In this paper, we have presented detailed numerical results (obtained from MC simulations) for the autocorrelation function $A_m(t,t_w)$, defined in Eq. (14). [Similar results are obtained for the other autocorrelation function $A_\rho(t,t_w)$, but we do not present these here for the sake of brevity.] In domain-growth processes, this quantity exhibits *aging* or dependence on the initial reference time $t_w$. Typically, the decorrelation process occurs due to two physical mechanisms: (a) equilibrium fluctuations in bulk domains, which correspond to a *stationary* or *nonaging* process, and (b) domain-wall motion, which corresponds to a *nonstationary* or *aging* process. There have been extensive studies of the autocorrelation function which characterizes either of these mechanisms, though these have been in the context of two-state kinetic Ising models.

In this paper, we present a stochastic model that accounts for both aging and nonaging contributions to the autocorre-

lation function. Our modeling is based on a Markovian description for single-spin dynamics coupled with the assumption that the relaxation times for a spin depend on the size of the domain to which it belongs. Our analytical results are in good agreement with the numerical results. Furthermore, in the long-time limit ($t\to\infty$), our theory is consistent with the Huse-Fisher scenario [28] for decorrelation due to bulk domain fluctuations.

The results discussed in this paper are obtained in the context of a spin-1 model, but the paradigm is rather general and readily applicable to the two-state kinetic Ising model and other spin models. We believe that the stochastic formulation presented here provides a fruitful way of understanding autocorrelation functions in phase-ordering systems.


## ACKNOWLEDGMENTS

The authors are grateful to K. Tafa for collaboration in the early stages of this work.


## APPENDIX: STOCHASTIC MODEL FOR AUTOCORRELATION FUNCTIONS

In this appendix, we present details of the calculation of spin-1 autocorrelation functions using the CTRW formalism [47–49]. We have already introduced the persistence matrix in Eq. (17) and the transition matrix in Eq. (18). Since it is not necessary that a transition occurs at $t=0$, the waiting-time distribution for the first spin transition is different from $\psi_n(t)$, and is given by [47–49]

$$\phi_n(t) = \frac{1}{\tau_n}\int_t^\infty dt'\,\psi_n(t'),\ \tau_n = \int_0^\infty dt\,\psi_n(t). \tag{A1}$$

Thus, the persistence and transition matrices for the first transition are obtained by replacing $\psi_n$ by $\phi_n$ in Eqs. (17) and (18):

$$\Psi_1(t) = \begin{pmatrix} \phi_+(t) & 0 & 0 \\ 0 & \phi_0(t) & 0 \\ 0 & 0 & \phi_-(t) \end{pmatrix},$$

$$W_1(t) = -\begin{pmatrix} 0 & \frac{1}{2}\dot{\phi}_0(t) & 0 \\ \dot{\phi}_+(t) & 0 & \dot{\phi}_-(t) \\ 0 & \frac{1}{2}\dot{\phi}_0(t) & 0 \end{pmatrix}. \tag{A2}$$

In the CTRW formalism, we can obtain the probability vector $\vec{P}(t)$, starting from $\vec{P}(0)$, by summing over different paths. These paths can be labeled by the number of transitions that occur in the interval $[0,t]$. The matrix corresponding to $n$ transitions is

$$U_n(t) = \int_0^t dt_n \int_0^{t_n} dt_{n-1}\cdots\int_0^{t_2} dt_1 \times \Psi(t-t_n)W(t_n-t_{n-1})\cdots W(t_2-t_1)W_1(t_1), \tag{A3}$$

valid for $n\geqslant 1$. Then, the state at time $t$ is

$$\vec{P}(t) = U(t)\vec{P}(0) = \left(\sum_{n=0}^{\infty} U_n(t)\right)\vec{P}(0), \tag{A4}$$

where we identify $U_0(t)=\Psi_1(t)$. The sum is performed by taking the Laplace transform of this equation, and one obtains

$$\tilde{\vec{P}}(s) = \left(\tilde{\Psi}_1(s) + \tilde{\Psi}(s)\frac{1}{1-\tilde{W}(s)}\tilde{W}_1(s)\right)\vec{P}(t=0) \equiv \tilde{U}(s)\vec{P}(t=0), \tag{A5}$$

where $\tilde{F}(s)$ denotes the Laplace transform, $\tilde{F}(s) = \int_0^\infty dt\, e^{-st}F(t)$.

The matrices which determine $\tilde{U}(s)$ can be written in terms of $\tilde{\psi}_n(s)$ as follows:

$$\tilde{\Psi}_1(s) = \frac{1}{s}I - \frac{1}{s}\begin{pmatrix} \frac{\tilde{\psi}_+}{\tau+} & 0 & 0 \\ 0 & \frac{\tilde{\psi}_0}{\tau_0} & 0 \\ 0 & 0 & \frac{\tilde{\psi}_-}{\tau_-} \end{pmatrix},$$

$$\tilde{\Psi}(s) = \begin{pmatrix} \tilde{\psi}_+ & 0 & 0 \\ 0 & \tilde{\psi}_0 & 0 \\ 0 & 0 & \tilde{\psi}_- \end{pmatrix},$$

$$\tilde{W}_1(s) = \begin{pmatrix} 0 & \frac{\tilde{\psi}_0}{2\tau_0} & 0 \\ \frac{\tilde{\psi}_+}{\tau_+} & 0 & \frac{\tilde{\psi}_-}{\tau_-} \\ 0 & \frac{\tilde{\psi}_0}{2\tau_0} & 0 \end{pmatrix},$$

$$\tilde{W}(s) = \begin{pmatrix} 0 & \frac{1}{2}(1-s\tilde{\psi}_0) & 0 \\ 1-s\tilde{\psi}_+ & 0 & 1-s\tilde{\psi}_- \\ 0 & \frac{1}{2}(1-s\tilde{\psi}_0) & 0 \end{pmatrix}, \tag{A6}$$

where $I$ is the $3\times 3$ unit matrix. This allows us to obtain the evolution operator as

$$\widetilde{U}(s)=\frac{1}{s}I-\frac{1}{s}\begin{pmatrix}\dfrac{\widetilde{\psi}_+}{\tau_+} & 0 & 0\\ 0 & \dfrac{\widetilde{\psi}_0}{\tau_0} & 0\\ 0 & 0 & \dfrac{\widetilde{\psi}_-}{\tau_-}\end{pmatrix}+\frac{1}{D}\begin{pmatrix}\dfrac{\widetilde{\psi}_+^2}{2\tau_+}(1-s\widetilde{\psi}_0) & \dfrac{\widetilde{\psi}_+\widetilde{\psi}_0}{2\tau_0} & \dfrac{\widetilde{\psi}_+\widetilde{\psi}_-}{2\tau_-}(1-s\widetilde{\psi}_0)\\ \dfrac{\widetilde{\psi}_+\widetilde{\psi}_0}{\tau_+} & \dfrac{\widetilde{\psi}_0^2}{2\tau_0}(2-s\widetilde{\psi}_+-s\widetilde{\psi}_-) & \dfrac{\widetilde{\psi}_0\widetilde{\psi}_-}{\tau_-}\\ \dfrac{\widetilde{\psi}_+\widetilde{\psi}_-}{2\tau_+}(1-s\widetilde{\psi}_0) & \dfrac{\widetilde{\psi}_0\widetilde{\psi}_-}{2\tau_0} & \dfrac{\widetilde{\psi}_-^2}{2\tau_-}(1-s\widetilde{\psi}_0)\end{pmatrix}, \tag{A7}$$

where

$$D=\det[1-\widetilde{W}(s)]=\frac{s}{2}(2\widetilde{\psi}_0+\widetilde{\psi}_++\widetilde{\psi}_-)-\frac{s^2}{2}\widetilde{\psi}_0(\widetilde{\psi}_++\widetilde{\psi}_-). \tag{A8}$$

Next, we consider the calculation of the autocorrelation functions. We have the definition

$$A_m(t)=\langle s(t)s(0)\rangle-\langle s(t)\rangle\langle s(0)\rangle=\left(\sum_{n,n_0=0,\pm1}nn_0P_{n|n_0}(t)P_{n_0}(0)\right)-\langle s(t)\rangle\langle s(0)\rangle. \tag{A9}$$

Here, the quantity $P_{n|n_0}(t)$ denotes the conditional probability for state $n$ at time $t$, provided that the spin was in state $n_0$ at $t=0$. For different $(n,n_0)$ values, these are identified as the matrix elements of $U(t)$. Furthermore, we will consider initial conditions where $\langle s(0)\rangle=0$. The only combinations that contribute to the sum in Eq. (A9) are those with $n$, $n_0=\pm1$. Thus, we have

$$A_m(t)=P_{+|+}(t)P_+(0)+P_{-|-}(t)P_-(0)-P_{+|-}(t)P_-(0)-P_{-|+}(t)P_+(0). \tag{A10}$$

For the spatially extended system, recall that we are interested in random initial states with probabilities $(1-c_V)/2$ of site $i$ being occupied by an $A$ or $B(s_i=\pm1)$, and $c_V$ of site $i$ being occupied by $V(s_i=0)$. Thus, we set

$$P_+(0)=P_-(0)=\frac{1-c_V}{2},\quad P_0(0)=c_V. \tag{A11}$$

This yields

$$A_m(t)=\frac{1-c_V}{2}(U_{11}+U_{33}-U_{13}-U_{31}). \tag{A12}$$

Similarly, we define

$$A_\rho(t)=\langle s^2(t)s^2(0)\rangle-\langle s^2(t)\rangle\langle s^2(0)\rangle=\left(\sum_{n,n_0=0,\pm1}n^2n_0^2P_{n|n_0}(t)P_{n_0}(0)\right)-\langle s^2(t)\rangle\langle s^2(0)\rangle. \tag{A13}$$

Following the above calculation, we obtain the final result

$$A_\rho(t)=c_V(1-c_V)\left(\frac{U_{11}+U_{13}+U_{31}+U_{33}}{2}-(U_{12}+U_{32})\right). \tag{A14}$$

Finally, we present explicit expressions for these functions when the $\psi_n$'s have an exponential form:

$$\psi_n(t)=e^{-\gamma_nt}=e^{-t/\tau_n},\quad \widetilde{\psi}_n(s)=\frac{1}{s+\gamma_n}. \tag{A15}$$

Then, some algebra yields the expression

$$\widetilde{A}_m(s)=\frac{1-c_V}{2}\left(\frac{1}{s+\gamma_+}+\frac{1}{s+\gamma_-}-\frac{\gamma_0(\gamma_+-\gamma_-)^2}{(s+\gamma_+)(s+\gamma_-)}\frac{1}{[2(s+\gamma_+)(s+\gamma_-)+\gamma_0(2s+\gamma_++\gamma_-)]}\right)=\frac{1-c_V}{2\gamma_r}\left(\frac{\gamma_r+\gamma_0}{s+\gamma_a}+\frac{\gamma_r-\gamma_0}{s+\gamma_b}\right), \tag{A16}$$

where

$$\gamma_{a,b}=\frac{(\gamma_0+\gamma_++\gamma_-)\mp\gamma_r}{2},\quad \gamma_r=\sqrt{(\gamma_+-\gamma_-)^2+\gamma_0^2}. \tag{A17}$$

Now, the inverse Laplace transform of $\widetilde{A}_m(s)$ is easily obtained as

$$A_m(t)=\frac{1-c_V}{2\gamma_r}[(\gamma_r+\gamma_0)e^{-\gamma_at}+(\gamma_r-\gamma_0)e^{-\gamma_bt}]. \tag{A18}$$

The corresponding expression for the other correlation function is obtained as follows:

$$\widetilde{A}_\rho(s)=\frac{c_V(1-c_V)}{2}\left[\frac{1}{s+\gamma_+}+\frac{1}{s+\gamma_-}-\frac{\gamma_0}{2}\left(\frac{(2s+\gamma_++\gamma_-)^2}{(s+\gamma_+)(s+\gamma_-)(s+\gamma_a)(s+\gamma_b)}\right)\right]=\frac{c_V(1-c_V)}{2\gamma_r}\left(\frac{\gamma_r-\gamma_0}{s+\gamma_a}+\frac{\gamma_r+\gamma_0}{s+\gamma_b}\right). \tag{A19}$$

Then, the inverse Laplace transform of $\widetilde{A}_\rho(s)$ is

$$A_\rho(t)=\frac{c_V(1-c_V)}{2\gamma_r}[(\gamma_r-\gamma_0)e^{-\gamma_at}+(\gamma_r+\gamma_0)e^{-\gamma_bt}]. \tag{A20}$$

[1] K. Binder, in *Phase Transformations of Materials*, Materials Science and Technology Vol. 5, edited by R.W. Cahn, P. Haasen, and E.J. Kramer, (VCH, Weinheim, 1991), p. 405.
[2] A.J. Bray, Adv. Phys. **43**, 357 (1994).
[3] A. Onuki, *Phase Transition Dynamics* (Cambridge University Press, Cambridge, U.K., 2002).
[4] S. Dattagupta and S. Puri, *Dissipative Phenomena in Condensed Matter Physics* (Springer, Berlin, 2004).
[5] K. Binder and D. Stauffer, Phys. Rev. Lett. **33**, 1006 (1974); Z. Phys. B **24**, 406 (1976).
[6] I.M. Lifshitz, Sov. Phys. JETP **15**, 939 (1962); S.M. Allen and J.W. Cahn, Acta Metall. **27**, 1085 (1979).
[7] I.M. Lifshitz and V.V. Slyozov, J. Phys. Chem. Solids **19**, 35 (1961).
[8] L.C.E. Struik, *Physical Aging in Amorphous Polymers and Other Materials* (Elsevier, Amsterdam, 1978).
[9] L. Lundgren, P. Svedlindh, P. Nordblad, and O. Beckman, Phys. Rev. Lett. **51**, 911 (1983); L. Lundgren, P. Nordblad, and L. Sandlund, Europhys. Lett. **1**, 529 (1986).
[10] R.V. Chamberlin, G. Mozurkewich, and R. Orbach, Phys. Rev. Lett. **52**, 867 (1984).
[11] J.-P. Bouchaud, L.F. Cugliandolo, J. Kurchan, and M. Mezard, in *Spin Glasses and Random Fields*, edited by A.P. Young, (World Scientific, Singapore, 1997), p. 161.
[12] A. Crisanti and F. Ritort, J. Phys. A **36**, R181 (2003).
[13] H. Rieger, B. Steckemetz, and M. Schreckenberg, Europhys. Lett. **27**, 485 (1994).
[14] J. Kisker, L. Santen, M. Schreckenberg, and H. Rieger, Phys. Rev. B **53**, 6418 (1996).
[15] M. Blume, V.J. Emery, and R.B. Griffiths, Phys. Rev. A **4**, 1071 (1971).
[16] D. Mukamel and M. Blume, Phys. Rev. A **10**, 610 (1974).
[17] J. Lajzerowicz and J. Sivardiere, Phys. Rev. A **11**, 2079 (1975); J. Sivardiere and J. Lajzerowicz, *ibid.* **11**, 2090 (1975); **11**, 2101 (1975).
[18] D. Furman, S. Dattagupta, and R.B. Griffiths, Phys. Rev. B **15**, 441 (1977).
[19] W. Hoston and A.N. Berker, Phys. Rev. Lett. **67**, 1027 (1991).
[20] S. Puri and D. Kumar, Phys. Rev. Lett. **93**, 025701 (2004).
[21] K. Yaldram and K. Binder, Z. Phys. B: Condens. Matter **82**, 405 (1991); J. Stat. Phys. **62**, 161 (1991); Acta Metall. Mater. **39**, 707 (1991).
[22] P. Fratzl and O. Penrose, Phys. Rev. B **50**, 3477 (1994); **53**, 2890 (1996).
[23] M. Plapp and J.-F. Gouyet, Phys. Rev. Lett. **78**, 4970 (1997); Eur. Phys. J. B **9**, 267 (1999).
[24] S. Puri, Phys. Rev. E **55**, 1752 (1997).
[25] S. Puri and R. Sharma, Phys. Rev. E **57**, 1873 (1998).
[26] K. Tafa, S. Puri, and D. Kumar, Phys. Rev. E **64**, 056139 (2001).
[27] K. Tafa, S. Puri, and D. Kumar, Phys. Rev. E **63**, 046115 (2001); Phase Transitions **75**, 413 (2002).
[28] D.A. Huse and D.S. Fisher, Phys. Rev. B **35**, 6841 (1987).
[29] K.L. Ngai and A.K. Rajagopal, in *Non-Debye Relaxation in Condensed Matter Physics*, edited by T.V. Ramakrishnan and M.R. Lakshmi (World Scientific, Singapore, 1987).
[30] J. Jäckle, Philos. Mag. B **56**, 113 (1987).
[31] H. Takano, H. Nakanishi, and S. Miyashita, Phys. Rev. B **37**, 3716 (1988).
[32] C. Tang, H. Nakanishi, and J.S. Langer, Phys. Rev. A **40**, 995 (1989).
[33] A.T. Ogielski, Phys. Rev. B **36**, 7315 (1987).
[34] I.S. Graham and M. Grant, J. Phys. A **25**, L1195 (1992).
[35] D.S. Fisher and D.A. Huse, Phys. Rev. Lett. **56**, 1601 (1986); Phys. Rev. B **38**, 373 (1988); **38**, 386 (1988).
[36] T. Ohta, D. Jasnow, and K. Kawasaki, Phys. Rev. Lett. **49**, 1223 (1982).
[37] R.J. Glauber, J. Math. Phys. **4**, 294 (1963).
[38] A.J. Bray, J. Phys. A **23**, L67 (1990).
[39] K. Humayun and A.J. Bray, J. Phys. A **24**, 1915 (1991).
[40] C. Yeung, M. Rao, and R.C. Desai, Phys. Rev. E **53**, 3073 (1996).
[41] J.F. Marko and G.T. Barkema, Phys. Rev. E **52**, 2522 (1995).
[42] K. Binder and A.P. Young, Rev. Mod. Phys. **58**, 801 (1986).
[43] M. Mezard, G. Parisi, and M. Virasoro, *Spin Glass Theory and Beyond* (World Scientific, Singapore, 1987).
[44] G. Parisi, Phys. Rev. Lett. **43**, 1754 (1979); J. Phys. A **13**, L115 (1980).
[45] D. Sherrington and S. Kirkpatrick, Phys. Rev. Lett. **35**, 1792 (1975).
[46] K. Binder and D.W. Heermann, *Monte Carlo Simulation in Statistical Physics: An Introduction*, 4th ed. (Springer-Verlag, Berlin, 2002).
[47] E.W. Montroll and G.H. Weiss, J. Math. Phys. **6**, 167 (1965).
[48] E.W. Montroll and H. Scher, J. Stat. Phys. **9**, 101 (1973).
[49] J.T. Bendler and M.F. Shlesinger, in *The Wonderful World of Stochastics*, edited by M.F. Shlesinger and G.H. Weiss (Elsevier, Amsterdam, 1985), p. 32.
[50] V.M. Kenkre and R.S. Knox, Phys. Rev. B **9**, 5279 (1974); V.M. Kenkre, *ibid.* **12**, 2150 (1975).
[51] J.W. Haus and K.W. Kehr, Phys. Rep. **150**, 263 (1987).